Spin-exchange optical pumping of ^{3}He with Rb-K mixtures and pure K

W. C. Chen and T. R. Gentile
National Institute of Standards and Technology, Stop 8461, Gaithersburg, Maryland 20899, USA

T. G. Walker and E. Babcock*
Department of Physics, University of Wisconsin-Madison, Madison, Wisconsin 53706, USA
(Received 25 September 2006; published 23 January 2007)

We have studied the efficiency of spin-exchange optical pumping (SEOP) in cells that contain either pure rubidium, mixtures of rubidium and potassium, or pure potassium. Optical pumping was performed with spectrally narrowed diode array lasers operating at either the wavelength of the Rb $5s_{1/2}$-$5p_{1/2}$ transition (795 nm) or the K $4s_{1/2}$-$4p_{1/2}$ transition (770 nm). Calculations of the expected efficiency are shown for practical conditions and compared to measurements. We have measured the vapor density ratio in Rb-K mixture cells using absorption of white light. Our focus is on the conditions that are relevant for neutron spin filters, but the results are relevant to all applications of SEOP. We find that both Rb-K and pure K cells yield improvements in the spin-exchange efficiency, and each approach has its own advantages. Overall, the best results for high polarizing rate with high polarization were obtained with mixture cells with K-Rb vapor density ratios between 2 and 6.

DOI: 10.1103/PhysRevA.75.013416 PACS number(s): 32.80.Bx

I. INTRODUCTION

Spin-exchange optical pumping (SEOP) of ^{3}He [1,2] is an important method in several areas of physics, including neutron spin filters for neutron scattering and fundamental neutron physics [3–5], spin-polarized targets [6,7], and magnetic resonance imaging [8]. In comparison to metastability-exchange optical pumping (MEOP) [9–11], SEOP is relatively simple, compact, and well suited to long-term, continuous operation because the gas can be directly optically pumped at the typical pressures of 1–10 bar needed for most applications. However, the polarizing rate of SEOP is much lower than that of MEOP, and the laser power requirements are much higher. As the gas volume and production rate needed for applications is increasing, this issue is of growing significance. In the SEOP method, electronic polarization is produced by optical pumping of Rb atoms, and the polarization is transferred to the ^{3}He nuclei by the hyperfine interaction during collisions. The efficiency of SEOP could be increased if potassium or sodium were used as the alkali-metal spin-exchange partner rather than rubidium, due to their lower electronic spin-destruction rates [1,12,13]. Nevertheless, Rb has remained the alkali-metal of choice primarily because of the availability of high-power diode lasers at the 795 nm wavelength of the Rb $5s_{1/2}$-$5p_{1/2}$ transition. Reported studies of direct optical pumping of potassium were performed with narrow band titanium sapphire lasers [13,14], which are now rarely employed for most applications because of the higher power, greater simplicity, smaller size, and lower cost of diode lasers. Although these results were encouraging, more practical application with broadband diode array lasers is not guaranteed to be successful because the 3.4 nm fine structure splitting of the $4s$-$4p$ transition in potassium is comparable to the typical linewidth of 2.5 nm [full width at half maximum (FWHM)] for such lasers. Recently, a method employing mixtures of Rb and K [15], with optical pumping of the Rb alone, was reported [16]. This hybrid method for SEOP yields most of the gain in efficiency possible for direct optical pumping of K but avoids the need for a new laser wavelength as well as the fine structure issue. In this paper, we report studies of both hybrid Rb-K spin-exchange optical pumping and direct optical pumping of K, and provide practical information for employing these approaches. In both cases, we employ spectrally narrowed diode array lasers [17] with linewidths of 0.2–0.3 nm FWHM. Although we focus on the needs of neutron spin filters, the results provide practical information for SEOP with Rb-K mixtures and pure K, which is relevant to all applications of polarized ^{3}He. We begin in Sec. II with calculations of the expected gain in efficiency and polarizing rate for practical application of hybrid and pure K cells, and compare to previous work. In Sec. III, we describe the apparatus used for our measurements and the methods we employed to characterize Rb-K mixtures. Section IV is divided into three parts; the first part covers SEOP of Rb-K cells at 795 nm, the second covers SEOP of pure K cells, and in the third part we compare 770 and 795 nm pumping of Rb-K cells. In Sec. V, we summarize the results of this study.

II. EFFICIENCY AND POLARIZING RATE COMPARISONS

A. Calculational methods

To discuss the utility of hybrid and pure K SEOP, we begin by defining the spin-exchange efficiency, which is the ratio of the rate at which nuclear spin-polarized gas is produced to the rate at which electronic spin-polarized alkali-metal vapor is destroyed

*Current address: Institut Laue-Langevin, B.P. 156, 38042 Grenoble, France.

$$\eta_A = \frac{\gamma_{se}^A[^3\mathrm{He}]}{\Gamma_A[A]}. \quad (1)$$

Here, $\gamma_{se}^A = k_{se}^A[A]$ is the spin-exchange rate from the alkali-metal A (Rb or K in this work) to the ^{3}He, k_{se}^A is the spin-exchange rate constant for the alkali-metal, $[A]$ is the number-density of the alkali-metal vapor, $[^3\mathrm{He}]$ is the density of ^{3}He, and Γ_A is the electronic spin-destruction rate for the alkali-metal. For Rb-K cells, the total spin-exchange rate (in Hz) is

$$\gamma_{se}^{\mathrm{Rb-K}} = k_{se}^{\mathrm{Rb}}[\mathrm{Rb}] + k_{se}^{\mathrm{K}}[\mathrm{K}]. \quad (2)$$

For optical pumping of the Rb, the spin-destruction rate (in Hz) is replaced by

$$\Gamma'_{\mathrm{Rb}} = \Gamma_{\mathrm{Rb}} + D\Gamma_{\mathrm{K}} + q_{\mathrm{KR}}[\mathrm{K}], \quad (3)$$

where $D=[\mathrm{K}]/[\mathrm{Rb}]$ is the vapor density ratio and q_{KR} is the spin-destruction rate constant for Rb-K collisions [16]. As discussed below, SEOP with pure K or Rb-K mixtures is more efficient than SEOP with pure Rb because k_{se}^{Rb} and k_{se}^{K} are comparable, whereas Γ_{K} is much smaller than Γ_{Rb}. In hybrid cells, rapid electronic spin-exchange between the K and Rb equalizes the polarization of the two alkali-metals, allowing for the benefits of the lower spin-destruction rate for K with no change in the optical pumping laser. The gain in efficiency relative to pure Rb depends on the vapor density ratio D.

To calculate these efficiencies, we used measured spin-exchange rate constants of $k_{se}^{\mathrm{Rb}}=6.8\times10^{-20}$ cm^3/s [18] and $k_{se}^{\mathrm{K}}=5.5\times10^{-20}$ cm^3/s [19], and the following expressions for the alkali-metal densities:

$$[\mathrm{Rb}]_0 = \left(\frac{7.25\times10^{16}}{T}\right)10^{9.318-4040/T}\ \mathrm{cm}^{-3}, \quad (4)$$

$$[\mathrm{K}]_0 = \left(\frac{7.25\times10^{16}}{T}\right)10^{9.408-4453/T}\ \mathrm{cm}^{-3}, \quad (5)$$

where the subscript 0 indicates the equilibrium density for the pure alkali-metal and T is the temperature in Kelvin [20]. These expressions were found to yield spin-exchange rates that agree with our observed rates within 10%. (The accuracy quoted for these formulas is ±5%.) For hybrid cells, we assume that the densities are approximately given by Raoult's Law [21], i.e., $[\mathrm{Rb}]\approx m_{\mathrm{Rb}}[\mathrm{Rb}]_0$, where m_{Rb} is the mole fraction of Rb. The vapor density ratio is then given by

$$D \approx S(T)\left(\frac{1-m_{\mathrm{Rb}}}{m_{\mathrm{Rb}}}\right), \quad (6)$$

where $S(T)=[\mathrm{K}]_0/[\mathrm{Rb}]_0$ is the ratio of the equilibrium vapor densities at a given temperature. D increases slowly with increasing temperature because of the different slopes of the equilibrium vapor pressure curves.

The total alkali-metal spin-destruction rate Γ_A is given by $\Gamma_A=\Gamma_{A\text{-}A}+\Gamma_{A\text{-}^3\mathrm{He}}+\Gamma_{A\text{-}\mathrm{N}_2}$, arising from A-A, A-^{3}He, and A-N_2 collisions, respectively. (Because of the high optical opacity of the alkali-metal vapor for typical spin-exchange optical pumping conditions, nitrogen is added to quench radiative emission from excited alkali-metal atoms [1].) For Rb, we used the following expressions for these contributions to the spin-destruction rate (in Hz), where all densities are in atoms per cubic centimeter:

$$\Gamma_{\mathrm{Rb\text{-}Rb}} = 4.2\times10^{-13}[\mathrm{Rb}], \quad (7)$$

$$\Gamma_{\mathrm{Rb\text{-}}^3\mathrm{He}} = 1.0\times10^{-29}T^{4.259}[^3\mathrm{He}], \quad (8)$$

$$\Gamma_{\mathrm{Rb\text{-}N_2}} = 1.3\times10^{-25}T^3[\mathrm{N}_2]. \quad (9)$$

$[^3\mathrm{He}]$ is 2.48×10^{19} cm^{-3} at 1 bar and room temperature (296 K). The values for $\Gamma_{\mathrm{Rb\text{-}Rb}}$ and $\Gamma_{\mathrm{Rb\text{-}}^3\mathrm{He}}$ were obtained from recent measurements [13]. The rate constant for $\Gamma_{\mathrm{Rb\text{-}N_2}}$ was obtained from a measured cross section of 2.0×10^{-22} cm^2 at 480 K [22], and a relative collision velocity of $v_{\mathrm{Rb}}(1+87/28)^{1/2}=6.9\times10^4$ cm/s, where $v_{\mathrm{Rb}}=3.4\times10^4$ cm/s is the thermal velocity of Rb at 480 K. This yields a rate constant of 1.4×10^{-17} cm^3/s. We have assumed an approximate scaling of T^3 for the alkali-metal–nitrogen spin-destruction rate based on the following experimental results and theoretical arguments. Two measurements have been reported for the cross section for Rb-N_2 collisions: 2.0×10^{-22} cm^2 at 480 K and 2.5×10^{-22} cm^2 at 520 K [22], which would imply that the cross section varies as $T^{2.8}$. Rb-^{3}He and Rb-Xe spin-destruction rates have been found to vary as $T^{4.259}$ [13] and $T^{1.2}$ [23], respectively. This difference in temperature dependence is expected based on the softer shape of the repulsive potential experienced by a Rb atom during a collision with ^{3}He as compared to Xe [1]. We expect that the repulsive potential for nitrogen will fall somewhere between these two extremes. The efficiency comparisons discussed below are not sensitive to the exact value chosen for the exponent in the temperature dependence for nitrogen.

For the contributions to the K spin-destruction rate (in Hz), we used

$$\Gamma_{\mathrm{K\text{-}K}} = 9.6\times10^{-14}[\mathrm{K}], \quad (10)$$

$$\Gamma_{\mathrm{K\text{-}}^3\mathrm{He}} = (5.5\times10^{-20} + 5.8\times10^{-31}T^{4.259})[^3\mathrm{He}], \quad (11)$$

$$\Gamma_{\mathrm{K\text{-}N_2}} = 7.0\times10^{-26}T^3[\mathrm{N}_2]. \quad (12)$$

The value for $\Gamma_{\mathrm{K\text{-}K}}$ was obtained from a recent measurement [22]. The rate constant for $\Gamma_{\mathrm{K\text{-}}^3\mathrm{He}}$ is the sum of spin-rotation and spin-exchange contributions. The spin-rotation portion was deduced to be 8.9×10^{-20} cm^3/s at 423 K by measuring the spin-destruction rate for K-^{4}He and scaling for the lower reduced mass of the K-^{3}He pair [24]. The total Rb-^{3}He spin-destruction rate has been reported to have a $T^{4.259}$ temperature dependence [13], which is almost completely dominated by the spin-rotation contribution. We have assigned the same temperature dependence for the spin-rotation contribution to K-^{3}He spin-destruction. To this spin-rotation contribution, we add the temperature-independent spin-exchange rate coefficient of 5.5×10^{-20} cm^3/s to find the total spin-destruction rate coefficient. The rate constant for $\Gamma_{\mathrm{K\text{-}N_2}}$ was obtained from a measured cross section of 7.9×10^{-23} cm^2

at 440 K [22], and a relative collision velocity of 7.6×10^4 cm/s. This yields a rate constant of 6.0×10^{-18} cm^3/s. We have assumed T^3 scaling for the same reasons as discussed above for Rb. We do not know of any measurements or calculations of the spin-destruction rate from Rb-K collisions. As a reasonable estimate, we assumed a rate constant of $q_{KR}=2.2\times10^{-13}$ cm^3/s, which is the geometric mean between the aforementioned Rb-Rb and K-K spin destruction rates.

B. Performance criteria

There are two distinct, but coupled, practical motivations for increasing spin-exchange efficiency. The first motivation is to increase the volume of polarized gas that can be produced for a given laser power. The second is to increase the production rate for a given volume of gas, by increasing the spin-exchange rate via higher operating temperature. Finally, we may consider polarizing the same volume of gas at the same rate, but with reduced laser power. For neutron spin filter applications, the highest possible polarization is generally required; hence, these benefits must be obtained without loss of ^{3}He polarization. We assume that the product $\Gamma_A[A]V$, where V is the volume of the cell, is fixed for a given level of available laser power.

To increase the cell volume, we assume that one will keep the spin-exchange rate fixed, and assume that the volume can be scaled by the increased efficiency. We will denote E_D to be the ratio of the spin-exchange efficiency η_A of a cell with vapor density ratio D to that of a pure Rb cell (∞ denotes the limit of a pure K cell).

To increase the spin-exchange rate, we assume that the volume is held constant. In this case, it is more appropriate to examine the denominator of the spin-exchange efficiency, $\Gamma_A[A]$ for a single alkali-metal cell or $\Gamma'_{Rb}[Rb]$ for a hybrid cell [see Eq. (1)], which we will refer to as the "laser power demand" because the ideal laser power per unit volume is proportional to this denominator. The rate can be increased until the laser power demand for the pure K or hybrid cell equals that of the pure Rb cell. (The required laser power has been found to be much higher than the ideal laser power [16], but if the ratio of the laser power empirically observed to be required to the ideal laser power is independent of the value of the denominator, this approach should be valid.) We will denote R_D to be the ratio of the polarizing rate for a cell with vapor density ratio D to that of a pure Rb cell, for the same laser power demand.

To reduce the required laser power, we assume that the spin-exchange rate is fixed as for the volume case, and that the possible reduction in laser power scales with the laser power demand (denominator). Since it is only the change in the laser power demand that yields an increase in the spin-exchange efficiency, the possible decrease in required laser power will be essentially the same as the possible increase in volume.

C. Calculational results

Figure 1 shows the variation of the calculated efficiencies and laser power demands with the spin-exchange rate for pure Rb, pure K, and Rb-K hybrid cells at 1 bar [Fig. 1(a)] and 8 bar [Fig. 1(b)] for which we have assumed 67 mbar of N_2. (The laser power demands have been multiplied by 1×10^{-19} cm^3 s so as to yield a convenient dimensionless parameter for display with the spin-exchange efficiencies.) Cold neutron spin filters are typically operated near 1 bar [25], while rapid production of polarized ^{3}He for magnetic resonance imaging is typically performed at 8 bar. In addition, 8 bar would be a reasonable pressure for a centralized facility for dispensing polarized ^{3}He for neutron spin filters. Each plot shows results for $m_{Rb}=0.0175$ and $m_{Rb}=0.15$, for which D increases from 8 to 13 and from 0.8 to 1.3, respectively, in the temperature range from 440 to 570 K. As expected, the efficiencies are increased, and the laser power demands decreased, for pure K and hybrid cells. For hybrid

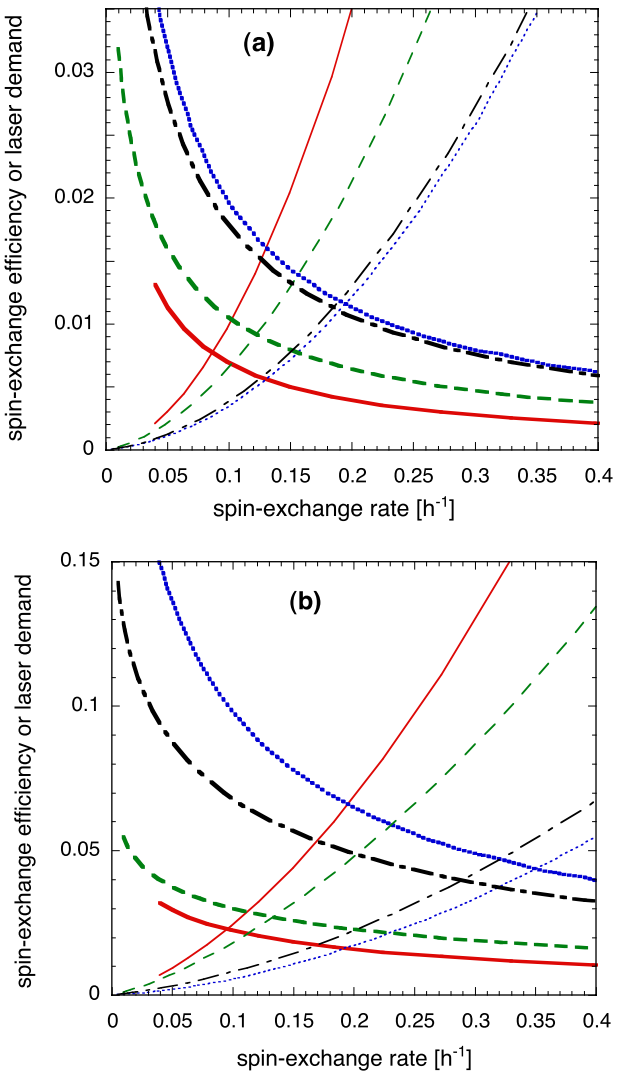

FIG. 1. (Color online) Calculated spin-exchange efficiencies (thick lines) and laser power demands (thin lines) (see Sec. II for definitions) for pressures of (a) 1 bar and (b) 8 bar, shown for pure Rb (solid red line), pure K (dotted blue line), $m_{Rb}=0.15$ (dashed green line, $D=0.8-1.3$), and $m_{Rb}=0.0175$ (dotted-dashed black line, $D=8-13$). (The laser power demands have been multiplied by 1×10^{-19} cm^3 s so as to yield a convenient dimensionless parameter for display with the spin-exchange efficiencies.)

cells, higher vapor density ratios yield the best performance. Since alkali-metal–alkali-metal spin destruction rates are larger than alkali-metal–buffer-gas spin-destruction rates for typical conditions, increasing the ^{3}He pressure increases the SEOP efficiency. The results are insensitive to the value of q_{KR} [see Eq. (3)]; setting it to zero only increases E_D by $\approx$15% at 1 bar or a few percent at 8 bar.

For typical spin-exchange rates of 0.1–0.2 h^{-1}, we observe that at 1 bar $E_\infty \approx 2.9$, $E_{10} \approx 2.6$, and $E_1 \approx 1.6$, whereas $R_\infty \approx 1.8$, $R_{10} \approx 1.7$, and $R_1 \approx 1.3$. At 8 bar $E_\infty \approx 4.3$, $E_{10} \approx 3.1$, and $E_1 \approx 1.4$, whereas $R_\infty \approx 2.5$, $R_{10} \approx 2.1$, and $R_1 \approx 1.2$. E_D and R_D were determined from the results shown in Fig. 1: for E_D we found the possible increase in spin-exchange efficiency for a given spin-exchange rate, whereas for R_D we found the possible increase in spin-exchange rate for a given laser power demand. For practical conditions, the dependence of E_D and R_D on spin-exchange rate is weak. At 1 bar, the possible improvement in rate is roughly equal to the square root of the possible improvement in volume (or reduction in laser power). This is because of the domination of spin-destruction from alkali-metal–alkali-metal collisions; since the laser power demand scales as the square of the alkali-metal density, the alkali-metal density (and thus the rate) can only be increased by the square root of the efficiency ratio. At 8 bar, the possible improvement in rate is closer to the possible improvement in volume (or reduction in laser power) due to the increasing role of alkali-metal–^{3}He spin-destruction. However, further increase in rate requires higher alkali-metal densities, thereby driving the operating point back towards domination by alkali-metal–alkali-metal rates. Hence, for a given pressure, the maximum efficiency is generally obtained by increasing the cell volume rather than the cell temperature, assuming experimental goals and mechanical constraints permit it.

In the limit where alkali-metal–alkali-metal spin-destruction completely dominates, we expect E_∞ evaluated at a given spin-exchange rate to be $4.4/1.23^2=2.9$, where 4.4 (1.23) is the ratio of the Rb-Rb and K-K spin-destruction rate constants (spin-exchange rate constants). In the case where alkali-metal–^{3}He spin-destruction dominates, we expect E_∞ evaluated for a typical spin-exchange rate of 0.1 h^{-1} to be $8.6/1.23=7.0$, where 8.6 is the ratio of the alkali-metal–^{3}He spin-destruction rate coefficients for Rb and K at temperatures of 453 and 502 K, respectively. We find that the calculated value of $E_\infty=2.9$ at 1 bar is close to that expected for complete domination by alkali-metal–alkali-metal spin-destruction, whereas the value of 4.3 at 8 bar results from contributions from both alkali-metal–alkali-metal and alkali-metal–buffer-gas relaxation. (In fact, alkali-metal–buffer-gas collisions have a non-negligible effect at 1 bar, but the effect of alkali-metal–N_2 collisions is to slightly decrease E_∞, whereas the effect of alkali-metal–^{3}He collisions is to slightly increase E_∞, and these effects roughly cancel.) The value of $E_\infty=7.0$ is observed in the limit of infinite ^{3}He pressure (for $\gamma_{se}=0.1$ h^{-1}).

At 1 bar, most of the possible gain is obtained with modest values of the vapor density ratio D. For high pressure, modest D yields only a fraction of the achievable gain; hence, ideally one would employ the highest D possible. However, it has been observed that the maximum achievable polarization decreases with increasing D [16]; as discussed below, we have also observed this behavior.

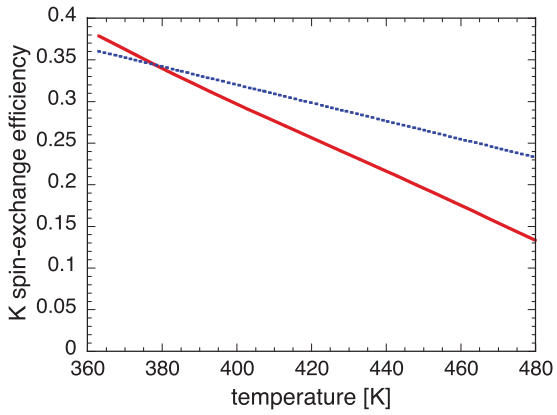

FIG. 2. (Color online) Variation of the calculated spin-exchange efficiency for K with temperature, for a ^{3}He pressure of 7.6 bar and a N_2 pressure of 0.1 bar (red solid line). The calculations in this work are compared to the fit of data in Ref. [13] (blue dotted line).

D. Comparison to reported results

In Fig. 2, we compare the variation of our calculated efficiencies for K with temperature to measurements that have been previously reported in the temperature range 360–475 K [13]. (By definition, our calculations agree well with those reported for Rb, as our calculations for Rb are based primarily on the spin-exchange and spin-relaxation rates reported in Ref. [13].) Our calculations for K show a steeper decline with increasing temperature than the measurements. Unfortunately, the measurements do not extend to the region in which the K vapor pressure is high enough for most practical applications (the spin-exchange rate is only 0.03 h^{-1} at the highest temperature of 475 K for which data were reported). If the reported weak dependence of the spin-exchange efficiency on temperature can be extrapolated to higher temperature, the potential improvement obtained with hybrid or pure K cells will be greater than our calculations indicate.

In the first demonstration of hybrid SEOP [16], a factor of 12 increase in the spin-exchange efficiency was reported for high D cells at a pressure of 8.7 bar, whereas our calculations yield an expected value of 4.1. However, in that work efficiencies were compared at a fixed temperature of 463 K, whereas our calculations are done for the same spin-exchange rate. At 463 K, the spin-exchange rate for Rb is 0.15 h^{-1}, whereas operation at 513 K is required to get the same value for K; between these two temperatures our calculated efficiency drops by a factor of 2.4, primarily due to increased K-K spin-destruction but also due to the temperature dependence of the alkali-metal–buffer-gas rates. Hence, if the spin-exchange rate is fixed, the factor of 12 decreases to $12/2.4=5.0$, somewhat larger than but, nevertheless, in fair agreement with our calculations. If, instead, one extrapolates the measurements of efficiency for K from Ref. [13] discussed above, a decrease of a factor of only 1.3 is expected between 463 and 513 K and the factor of 12 would only be decreased to 9.2.

TABLE I. ^{3}He cells used in this work, with vapor density ratio D (zero indicates pure Rb and ∞ indicates pure K) and the maximum values of the ^{3}He polarization, P_{He}, obtained in each cell. All cells are cylindrical, with diameter d and length l in centimeters, volume V in cubic centimeters, ^{3}He partial pressure p in bar, and relaxation time T_1 in hours. The cells and optical pumping conditions are described in the text. The results for optical pumping at 795 nm were obtained with 52 W of spectrally narrowed laser light from two diode bars. The results for optical pumping at 770 nm were obtained with 21 W of spectrally narrowed laser light from a single diode bar, except for the Chardonnay and Orvieto cells, for which data were obtained with 12 W. Because of time constraints, data with the 770 nm lasers were not obtained for all cells.

Cell	D	d	l	V	p	T_1	$P_{He}(795)$	$P_{He}(770)$
Chardonnay	1.6	8.4	7.3	400	1.07	390	0.77	0.67
Orvieto	2.2	8.7	7.2	430	1.1	80	0.70	0.63
Zinfandel	1.0	11.6	8.9	940	1.86	330	0.78	
Chianti	2.0	11.8	8.1	875	1.82	290	0.75	
Barbera	4.4	11.8	7.5	820	1.52	310	0.76	
Syrah	6.2	10.2	9.7	790	1.43	450	0.76	0.73
Riesling	4.8	9.8	9.0	680	3.5	170	0.77	0.68
Cabernet	46	11.8	7.6	830	1.94	270	0.58	0.71
Gigantor	96	9.1	9.4	611	0.85	800	0.56	0.73
Quasimoto	155	6.7	5.8	205	1.12	550	0.48	0.76
Sonora	∞	4.5	4.3	68	0.81	500		0.77
Wilma	0	4.9	4.9	91	0.9	830	0.76	
Chekhov	0	8.1	6.0	309	1.27	340	0.79	
Bullwinkle	0	6.9	7.1	268	1.22	550	0.72	
Dino	0	10.6	5.1	450	0.85	530	0.75	
Kirk	0	10.5	7.2	620	0.80	740	0.77	

III. APPARATUS

A. Cells

The sealed cells for this work were blown from GE180 [26] glass and filled at the National Institute of Standards and Technology (NIST) in Gaithersburg, Maryland, using techniques described previously [25]. To produce hybrid cells, a "Y-junction" is included in the glass manifold so that Rb and K can be distilled into individual arms that merge into the main manifold. A small amount of Rb is distilled into each cell several times so that a thin layer of Rb film is eventually visible in each cell. A small amount of potassium is then distilled into each cell several times. The vapor density ratio is not well controlled in this process, but the experience gained in making several cells of widely varying D has allowed us to improve the control. (It may be possible to use a chemical approach to obtain more controlled vapor density ratios, but we have not yet employed this approach [27,28].) Table I lists the parameters for the cells used in this work, which include pure Rb cells, hybrid Rb-K cells, and pure K cells. The cells are identified by the names listed in Table I. Measurement of D is discussed in Sec. III C below.

B. Lasers

Measurements were performed using the SEOP apparatus at the National Institute of Standards and Technology that has been described earlier [29]. Two 795 nm, spectrally narrowed diode lasers, each employing a 50 W diode bar [30], illuminated the cells from opposite sides. A total of 52 W of laser light was incident on the SEOP oven. As noted below, sometimes only one laser was used, and/or the power level of each laser was reduced. The linewidth of each laser was measured with an optical spectrometer with a resolution of 0.07 nm [31]; for one laser we observed a symmetric lineshape with a linewidth of 0.21 nm FWHM and a spectrally narrowed output power of 27 W, whereas for the other we obtained an asymmetric line shape with a linewidth of 0.30 nm and a spectrally narrowed output power of 25 W.

For direct optical pumping of K we constructed two spectrally narrowed diode lasers operating at 770 nm. One is based on a 20 W diode bar [32] and the other is based on a 40 W diode bar [33]. We obtained 12 and 21 W of laser light into the oven for the 770 nm lasers based on the 20 and 40 W bars, respectively. As shown in Fig. 3(a), we obtained a symmetric line shape with a linewidth of 0.21 nm FWHM for the laser based on the 20 W bar. The small peak at 768.6 nm is due to incomplete suppression of the unnarrowed spectrum, which was temperature tuned as high as we thought was safe by operating the laser's cooling water at 24 °C (at the maximum laser power). The issue of possible undesired optical pumping of the K $4s_{1/2}$-$4p_{3/2}$ transition is discussed below. The linewidth of the laser based on the 40 W bar was 0.26 nm FWHM, as shown in Fig. 3(b).

C. Vapor density measurement

To measure the vapor density ratio of hybrid cells, we illuminated the cell with a 50 W halogen spot light and used

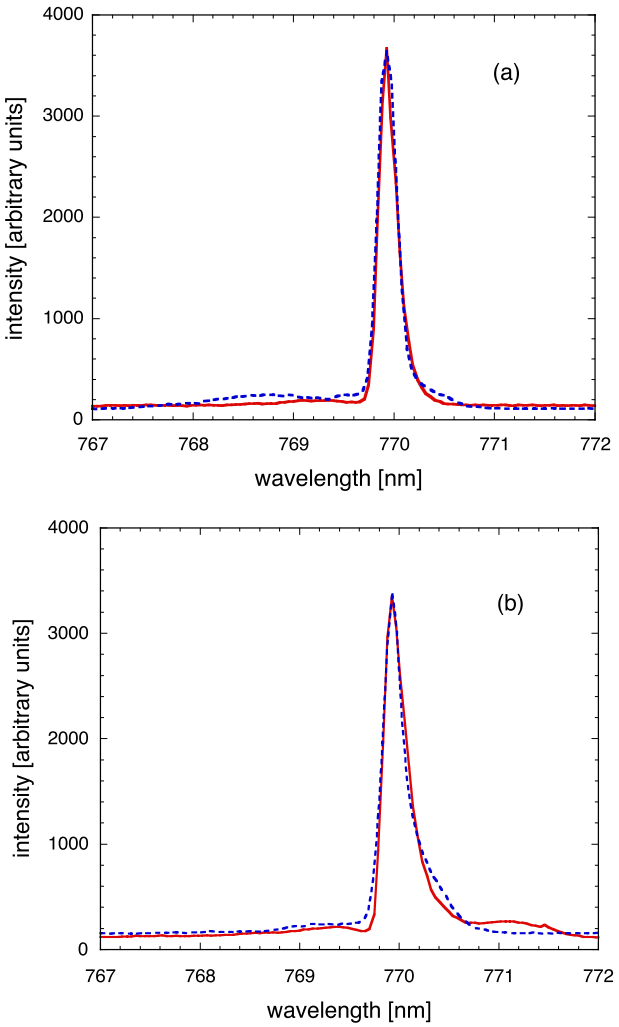

FIG. 3. (Color online) The spectra for the optical pumping comparisons in Sec. IV C. The spectra of the 795 nm lasers have been shifted to the same center as the 770 nm laser, and the peak heights have been normalized. (a) The spectrum for the 770 nm laser based on the 20 W bar (blue dotted line), and the 795 nm laser operated at the same output power (red solid line). Both linewidths are 0.21 nm FWHM. (b) The spectrum of the 770 nm laser based on the 40 W bar (blue dotted line), and the 795 nm laser operated at the same output power (red solid line). Both linewidths are 0.26 nm FWHM. The offsets of the data from zero are due to instrumental background.

the aforementioned optical spectrometer to measure the ratio of the absorption for K and Rb for each fine-structure transition. The temperature of the cell was adjusted so as to obtain dips in the transmission of 10–40%. The vapor density ratio at that temperature, labeled D_w in Table II, was determined from the ratio of the area of the dips. D_w was then corrected for operation at our actual operating temperatures for SEOP. This correction depends only on the variation in the ratio of the Rb and K vapor pressures with temperature, not the absolute vapor pressures. Nevertheless, this ratio can vary by a factor of two for different published vapor pressure formulas. Since we find agreement within 10% between the calculated and observed spin-exchange rates for pure Rb and K cells using Eqs. (4) and (5) for the vapor pressures, we employed these expressions to obtain values of the vapor density ratio at our operating temperatures (labeled D in Table II). For large D cells, we had to measure the dip areas for Rb and K at two different temperatures, hence different corrections based on Eqs. (4) and (5) were applied to obtain D. The relative standard uncertainties in Table II include a contribution of 10% from the uncertainties in the vapor pressure formulas we employed.

TABLE II. Determinations of the vapor density ratio D. For cells of moderate D, D_w is the value obtained at temperatures near 360 K using the white-light method discussed in the text. For the high-D Cabernet, Gigantor, and Quasimoto cells, the temperatures were increased to 413, 423, and 443 K, respectively, to obtain a measurable dip in transmission for Rb. D was obtained by correcting the results from the white-light method to the temperature for optical pumping, typically between 463 and 483 K. The values in parentheses are the uncertainties in the last digit(s). D_r is the range of values determined from polarizing rate measurements.

Cell	D_w	D	D_r
Chardonnay	0.8	1.6(4)	0.5–1.8
Orvieto	1.2	2.2(3)	1.8–2.7
Zinfandel	0.6	1.0(2)	0.6–0.8
Chianti	1.1	2.0(3)	1.2–1.8
Barbera	2.5	4.4(5)	2.7–5.3
Syrah	3.6	6.2(9)	4.7–5.9
Malbec	2.2	4.6(2)	3.8–4.7
Riesling	2.8	4.8(5)	2.6–5.8
Cabernet		46(7)	8–∞
Gigantor		96(22)	
Quasimoto		155(25)	14–∞
NHRbK	0.7	1.3(2)	

Table II lists the values of D_w and D determined using this method. We also checked the measured absorption ratio for the Rb $5s_{1/2}$-$5p_{3/2}$ (hereafter, referred to as Rb D_2) and $5s_{1/2}$-$5p_{1/2}$ (Rb D_1) transitions and the K $4s_{1/2}$-$4p_{3/2}$ (K D_2) and $4s_{1/2}$-$4p_{1/2}$ (K D_1) transitions, both of which are expected to be equal to 2.0 [34]. We measured 1.7±0.2 for Rb and 1.9±0.1 for K, in reasonable agreement with the expected value. The values of D_w in Table II are based on the average of those determined using the two fine structure transitions, and the uncertainties listed encompass both values. Faraday rotation [16] was employed at the University of Wisconsin to determine the vapor density ratio to be 170±10 for the Quasimoto cell and 1.5±0.1 for the cell NHRbK [35], confirming the results from the white-light method.

We also estimated the vapor density ratio based on the observed pumping rate for a given temperature. For hybrid pumping the spin-exchange rate $\gamma_{se}^{Rb\text{-}K}$ is given by Eq. (2), whereas for pure Rb pumping it is given by $k_{se}^{Rb}[Rb]_0$. Using Eq. (6) we obtain a rate-based estimate for the vapor density ratio (labeled D_r in Table II)

$$D_r = \frac{k_{se}^{Rb}[Rb]_0 - \gamma_{se}^{Rb\text{-}K}}{\gamma_{se}^{Rb\text{-}K}/S(T) - k_{se}^{K}[Rb]_0}. \quad (13)$$

D_r was evaluated using experimentally determined values of $\gamma_{se}^{Rb\text{-}K}$ (see Sec. IV), the equilibrium vapor densities from Eqs. (4) and (5), and known spin-exchange rate coefficients (see Sec. II A). The temperature was measured with a platinum resistance temperature device that was located under the cell. The range of values for D_r extracted from several pumps of each cell are listed in Table II. This approach is less accurate than, but generally in agreement with, the white-light method described above. Hence, we do not observe any significant deviations from the form of the vapor density ratio assumed in Eq. (6). If D is larger than about ten, then the uncertainty in D_r becomes large.

We found that the vapor density ratio can change during the first few times that a cell is optically pumped. This was observed via both the white-light and the time constant methods. For example, D increased from 1.3 to 2.7 in the Chianti cell, and from 1.0 to 2.5 in the Zinfandel cell. We presume that these shifts occur because the Rb-K alloy is not fully mixed.

Improved accuracy from the white-light method should be possible using the $4s$-$5p$ transitions for K (404.41 nm and 404.72 nm) and the $5s$-$6p$ transitions in Rb (420.18 and 421.55 nm). These transitions have on the order of 100 times weaker absorption than those we employed [36] and, thus, should allow for measurements at temperatures at or near those used for optical pumping.

IV. RESULTS

We report the achievable polarization and polarizing rate for hybrid and pure K cells, and make two comparisons to pure Rb cells: the maximum polarizing rate and the volume that can be polarized for a given laser power. Here "maximum" is defined as the highest rate at which the cell could be polarized without observing a decrease in alkali-metal polarization of more than 2%. To compare the maximum polarizing rates, we measured the variation of the initial pumping rate with temperature, typically in steps of 5 K or less. The initial rate is given by $\gamma_{se}^{A}P_A$, where P_A is the alkali-metal polarization, hence P_A can be determined if the initial rate is measured and γ_{se}^{A} is known. We first determined the spin-exchange rate at one or more temperatures using $\gamma_{se}^{A}=(\tau_{up}^{-1}-T_1^{-1})/(1+X)$, where the pumping time constant τ_{up} and the room-temperature relaxation time T_1 are measured and X is determined from measurements at sufficiently low temperature and/or sufficiently high laser power to observe saturation of the alkali-metal polarization [37]. X is a phenomenological parameter that reflects the observation that the slope of the ^{3}He relaxation rate vs alkali-metal density is greater than the spin-exchange rate [29,37]. For some of the hybrid cells, we compared results for optical pumping for 795 and 770 nm; in this case, we checked that the spin-exchange rates for a given temperature agreed within 10%. To determine the spin-exchange rates at other temperatures, we used Eqs. (4) and (5) to determine the change in the spin-exchange rate with respect to that measured for the temperature(s) at which we performed a full pumping curve. Note that we rely only on the shape of the vapor pressure curves, not the absolute values.

Except for high D cells, where there is evidence that the alkali-metal polarization is limited for 795 nm pumping (see below), we assume that the saturated value of the alkali-metal polarization is unity. For high D and pure K cells, X was determined from measurements obtained with the 770 nm laser. For all of the cells in this study, X was between 0.2 and 0.3. The surface to volume ratio for the cells in this study range betweeen 0.6 and 1.2 cm^{-1}. The values of X that we have observed are typical for cells of small surface to volume ratio [37]. The values of ^{3}He polarization, P_{He}, obtained with the maximum laser power available (52 W at 795 nm or 21 W at 770 nm) are listed in Table I and discussed below. P_{He} was determined with a typical relative standard uncertainty of 4% from nuclear magnetic resonance measurements that were calibrated against neutron transmission [29].

The actual gas temperature in spin-exchange cells can be higher than the temperature of the cell wall, due to the conversion of optical power to heat by the nitrogen buffer gas [38]. For much of this work, we compare results obtained for optical pumping of cells of similar geometry and ^{3}He pressure with the same level of laser power; hence, our results should not be sensitive to such effects. In addition, our studies are generally for optical pumping of large cells to high alkali-metal polarization (and thus weak optical absorption) with relatively low optical intensities; under these conditions we expect these effects to be modest. Furthermore, alkali-metal densities are determined by the temperature of the cell wall and alkali-metal–alkali-metal spin-destruction rates depend only on these densities. (Even if the rate coefficient has any temperature dependence, it would be weak.) By these arguments the only process in our cells that would be substantially modified by a difference between the gas and wall temperatures is spin destruction from alkali-metal–buffer-gas collisions, which have a strong temperature dependence. This modification could influence the data and modeling for the decline in alkali-metal polarization with increasing spin-exchange rate presented in Sec. IV C. However, we expect the influence to be small due to the dominance of spin-destruction from alkali-metal–alkali-metal collisions over most of the parameter regimes studied.

A. SEOP of Rb-K and pure Rb cells at 795 nm

Figure 4 shows the variation in alkali-metal polarization with spin-exchange rate for 795 nm pumping of two sets of cells that have similar volume and pressure: (i) Chekhov (D=0) and Chardonnay (D=1.6), and (ii) Chianti (D=2.0) and Barbera (D=4.4). These data were acquired with 52 W of 795 nm laser light. For these cells, the alkali-metal polarization is presumed to be unity at low spin-exchange rates. Comparison of the spin-exchange rate at which the alkali-metal polarization deviates from unity yields values for R_D. We estimate that the relative standard uncertainties for both the spin-exchange rates and the alkali-metal polarizations is 5%. However, the stability of the alkali-metal polarization

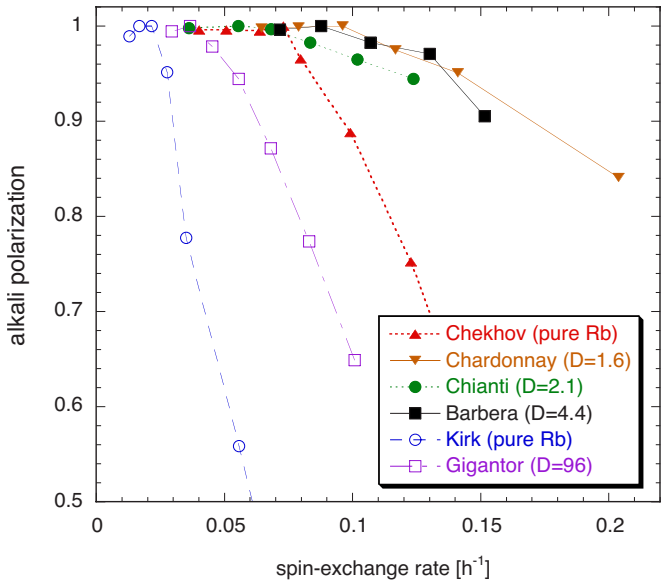

FIG. 4. (Color online) The variation in alkali-metal polarization with spin-exchange rate for three sets of cells that have similar volume and pressure. For 795 nm, pumping data are shown for (1) the Chekhov cell (pure Rb, solid upward triangles) and the Chardonnay cell (D=1.6, solid downward triangles) and (2) the Chianti cell (D=2.0, solid circles) and the Barbera cell (D=4.4, solid squares). Data are also shown for 770 nm pumping of the Gigantor cell (D=96, open squares) as compared to 795 nm pumping of the Kirk cell (pure Rb, open circles). Error bars are not shown to simplify the plot, but uncertainties are discussed in Sec. IV A. The lines are drawn to guide the eye.

measurements at low spin-exchange rates indicates that the precision in the alkali-metal polarization measurements is smaller than the absolute accuracy. We estimate the relative standard uncertainty in our determinations of R_D to be 10%.

For the comparison of the Chardonnay cell to the Chekhov cell, we find $R_{1.6}$=1.32, somewhat larger than the calculated value of 1.21. The calculated value was determined by the method described in Sec. II C, with a correction for the difference in cell volumes. For the cells Chianti and Barbera, the data represent a comparison of hybrid cells with different values of D. (Although less sensitive than a comparison to pure Rb, this approach was taken because we did not construct any pure Rb cells of this size and pressure.) Table III compares calculations and measurements of the ratios of maximum polarizing rate for sets of similar cells. The fairly modest improvements in polarizing rate for this regime of low pressures and low vapor density ratios require careful measurements. We generally find that the data show greater improvement as compared to the calculations. We observe that the decrease in alkali-metal polarization with increasing spin-exchange rate is more gradual for Rb-K cells as compared to either the pure Rb cell (Chekhov) or the nearly pure K cell (Gigantor; data obtained with 21 W of 770 nm laser light).

To illustrate the increase in gas volume that can be polarized, we considered data obtained for cells of similar pressure at similar spin-exchange rate and laser power. Using 12 W of laser light with a linewidth of 0.2 nm, we

TABLE III. Comparison of calculations (labeled *calc*) and measurements (labeled data) of the maximum polarizing rate for sets of similar cells. For the Chardonnay-Chekhov comparison, there are two listings, which were performed at different laser power. In several cases, we compare mixture cells of differing D, and thus list the ratio R_{D_1}/R_{D_2}, where D_1 and D_2 are the vapor density ratios for the higher and lower D cells, respectively. In these cases, we also list the calculated value of R_{D_1}. All cells were pumped at 795 nm, except Sonora and Gigantor, which were pumped at 770 nm. We estimate the relative standard uncertainty in our determinations of R_D to be 10%.

				R_{D_1}/R_{D_2}		R_{D_1}
Cell 1	Cell 2	D_1	D_2	data	*calc*	*calc*
Chardonnay	Chekhov	1.6	0	1.32	*1.21*	
Chardonnay	Chekhov	1.6	0	1.29	*1.20*	
Chardonnay	Dino	1.6	0	1.83	*1.48*	
Barbera	Chianti	4.4	2.0	1.28	*1.25*	*1.59*
Syrah	Chianti	6.2	2.0	1.32	*1.32*	*1.62*
Barbera	Zinfandel	2.5	1.0	1.69	*1.48*	*1.59*
Syrah	Zinfandel	6.2	1.0	1.75	*1.59*	*1.62*
Sonora	Wilma	∞	0	1.38	*2.02*	
Gigantor	Kirk	96	0	2.00	*1.87*	

obtained P_{He}=0.61 in the Bullwinkle cell (270 cm^3) with a spin-exchange time constant of 0.033 h^{-1}. This polarization value was limited by laser power. For the hybrid Syrah cell (D=6.2), which is 2.9 times larger in volume, we obtained a similar polarization value (P_{He}=0.65) for similar optical pumping conditions. We calculate an expected increase in efficiency of a factor of 2.0 for the Syrah cell as compared to the Bullwinkle cell; hence, we observe better performance than the calculation.

In summary, we observe increases in efficiency for 795 nm pumping of Rb-K cells that are generally somewhat better than our calculations. We find that for typical cold and/or thermal neutron spin filter pressures of 1–2 bar and D=2–6, the gain in efficiency from hybrid cells is up to a factor of three. Hence, the volume that can be polarized for a given laser power may be tripled, or the rate at which a given volume can be polarized is increased by up to a factor of $\approx$1.7.

For the Riesling cell (3.5 bar, 0.7 l, D=4.8), we were able to maintain full alkali-metal polarization with a 6.0 h pumping time constant, for 52 W of spectrally narrowed laser light. This allows for the production of 2.4 bar l/d of 75% polarized ^{3}He gas, assuming optical pumping for four time constants so as to reach 98% of the maximum ^{3}He polarization. For applications such as polarized gas magnetic resonance imaging, which can accept lower ^{3}He polarization, one can operate at shorter pumping time constants and/or stop the optical pumping earlier. For a 4.0 h pumping time constant, the maximum ^{3}He polarization was 66%, which would allow 2.4 bar l of 50% polarized ^{3}He gas to be produced in only 6 h. We have not constructed a similar pure Rb cell for comparison, but discuss 770 nm pumping of this cell in Sec.

IV C. Calculation of the expected gain in efficiency compared to pure Rb for $\gamma_{se}=5\ h^{-1}$ yields $E_{4.8}=2.5$ and $R_{4.8}=1.8$.

Based on the calculations, the efficiency should increase with higher vapor density ratios. However, we find that the maximum ^{3}He polarization decreases as D is increased. Whereas we obtained 76% ^{3}He polarization for the Syrah cell ($D=6.2$), the maximum ^{3}He polarization was reduced to 58% for the Cabernet cell ($D=46$) and 48% for the Quasimoto cell ($D=155$). A decrease in maximum alkali-metal polarization was observed in the initial work with hybrid cells [16] that employed broadband lasers. Hence, we assume that the alkali-metal in high-D Rb-K mixture cells cannot be fully polarized even with spectrally narrowed laser light at 795 nm. This hypothesis was confirmed by SEOP of these cells at 770 nm, which is discussed in Sec. IV B.

B. SEOP of pure K cells at 770 nm

Direct optical pumping of K at 770 nm should allow for increased efficiency as compared to pure Rb, avoid the issue of declining polarization in high-D Rb-K cells, and simplify alkali-metal distillation procedures in cell fabrication. To compare results obtained using the 770 nm laser to those obtained using the 795 nm laser, we must consider possible differences in the optical pumping efficiency itself. As shown in Fig. 3, the lineshape of the 770 nm laser based on the 20 W (40 W) bar is very similar to that of the 795 nm laser, when the 795 nm laser was operated at the same 12 W (21 W) power level of the 770 nm laser. The oscillator strength of the K D_1 transition is 3% smaller than the Rb D_1 transition [34], and the number of photons for a given laser power is 3% lower. These small effects would only reduce the optical pumping efficiency by $\approx$6%. The absorption width of the K D_1 line [39] has been reported to be 30% smaller than that of the Rb D_1 line [40]; hence, the absorption cross section on resonance is higher for K than for Rb. For weak absorption (fully polarized alkali-metal), this should not have any substantial effect. However, if the alkali-metal density is raised to increase the polarizing rate, the resonant light will be depleted slightly more rapidly in passage through the cell. Finally, we note that it has been observed that the photon efficiency for 795 nm pumping of Rb has been observed to be lower than expected [16]. Since this phenomenon is not understood, it could be larger or smaller for 770 nm pumping of K.

Another issue for 770 nm pumping is the small fine structure splitting (3.4 nm) in K, as optical pumping of the K D_2 transition will also reduce the optical pumping efficiency. Before we optimized the alignment of the 770 nm laser based on the 20 W bar, the height of the unsuppressed broadband peak at 768.6 nm was 15–20 % of the height of the narrowed peak, and under these conditions we found that we were only able to achieve ^{3}He polarization of 59% for the small, pure K Sonora cell. On reducing the unsuppressed peak to the level shown in Fig. 3(a), we have achieved 77% ^{3}He polarization. Small variations in the spectrum no longer appear to affect our results, but it is difficult for us to determine if they are negligible.

We also performed another test that is relevant to the possible use of broadband lasers for direct SEOP of K. The broadband peak for the 770 nm laser based on the 40 W bar (1.6 nm FWHM) was tuned to the K D_1 transition, with the grating mistuned to prevent narrowing. For the Sonora cell, the maximum ^{3}He polarization we could obtain with 21 W incident on the oven was 65%. Decreasing the oven temperature did not improve the alkali-metal polarization, hence the polarization may be limited by pumping of the D_2 transition.

Table III compares measured and calculated values of R_∞ for two different cell sets. We observed that the maximum rate was increased by a factor of only 1.38 for the pure K Sonora cell as compared to the pure Rb Wilma cell. Our calculation predicts a significantly higher value of 2.02. However, the maximum rate for the nearly pure K Gigantor cell ($D=96$) was increased by a factor of 2.0 as compared to the pure Rb Kirk cell (see Fig. 4), in close agreement with the calculated value of 1.87. For the Gigantor cell, we can also make a comparison of the volume that can be polarized for a given laser power similar to that discussed above for the Bullwinkle and Syrah cells. The Gigantor cell is similar in pressure but 2.3 times larger in volume than the Bullwinkle cell. We find that at nearly the same spin-exchange rate of 0.045 h^{-1}, we obtained $P_{He}=0.63$, close to that obtained in the Bullwinkle cell. We calculate that the increase in efficiency for the Gigantor cell as compared to the Bullwinkle cell should be a factor of $E_\infty=2.7$, in reasonable agreement with the measurements.

In addition to efficiency studies, we obtained additional information from direct SEOP at 770 nm. The maximum polarization values of 77% and 76% for the small Sonora and Quasimoto cells, respectively (see Table I), indicate that the same limit that has been observed for SEOP at 795 nm in pure Rb and hybrid cells [37] is operative for SEOP at 770 nm in pure K and hybrid cells. Note that the polarizations listed in Table I were lower for the Chardonnay and Orvieto cells because they were optically pumped with 12 W of 770 nm laser light, which did not provide sufficient power to yield unity alkali-metal polarization. Similarly, for the large Cabernet, Gigantor, Riesling, and Syrah cells we could only approach unity alkali-metal polarization at low temperature; hence, we suffered a small loss due to rate balance between spin-exchange and relaxation. For these cells, we plan future tests with increased laser power at 770 nm. The higher polarization values obtained by 770 nm pumping of cells of high vapor density ratio confirm the conclusion in previous studies [16] that the alkali-metal polarization is limited when such cells are optically pumped at 795 nm. In those studies, it was proposed that the decrease in alkali-metal polarization with increasing D could be due to off-resonant optical pumping of the potassium by the 795 nm laser. A value of $R_K/R=0.0027$ was determined, where R_K/R is the ratio of the optical pumping rate of the K atoms by 795 nm light to that of the Rb atoms. Based on the maximum alkali-metal polarization of 0.65 that we observed for 795 nm pumping of the Quasimoto cell, we determined a comparable value of $R_K/R=0.0036$. (Whereas a maximum attainable alkali-metal polarization, P_∞, was also included to analyze the results in Ref. [37], we fixed P_∞ to unity.)

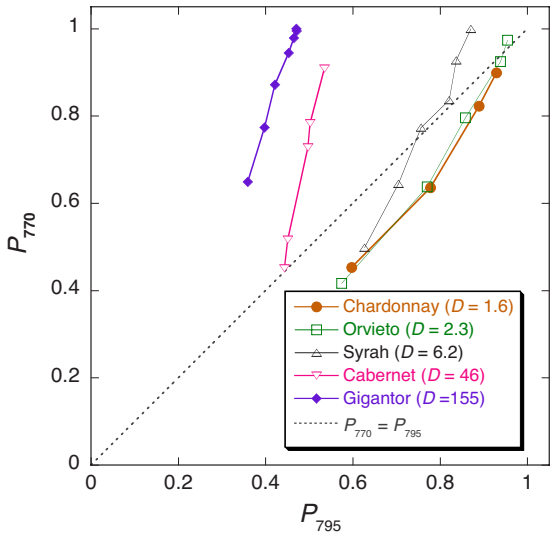

FIG. 5. (Color online) Comparison of the alkali-metal polarization obtained for 770 nm pumping at a given spin-exchange rate, P_{770}, and the alkali-metal polarization obtained for 795 nm pumping at the same spin-exchange rate, P_{795}, for the same laser power and linewidth. For the Chardonnay (solid circles) and Orvieto cells (open squares), the P_{770} data were obtained using the 770 nm laser based on the 20 W bar, whereas for the larger Syrah (upward, open triangles), Cabernet (downward, open triangles), and Gigantor cells (solid diamonds), the 40 W bar was employed. The dotted diagonal line shows $P_{770}=P_{795}$. To simplify the plot error bars are not shown, but uncertainties are discussed in Sec. IV A. The lines are drawn to guide the eye.

C. Comparison of optical pumping of hybrid cells at 795 and 770 nm

An additional study that we performed was to compare the achievable alkali-metal polarization obtained for SEOP of hybrid cells at 795 and 770 nm. The motivation for this study was to obtain further information about the relative optical pumping efficiencies. Both the 795 and 770 nm lasers were operated such that the same optical power was delivered to the cell from one side: when the 770 nm laser based on the 20 W bar was used, this power level was 12 W, whereas when the 770 nm laser based on the 40 W bar was used, the power level was 21 W. As shown in Fig. 3, the spectra were quite similar. These data are summarized in Fig. 5, in which the alkali-metal polarization obtained for 770 nm pumping at a given spin-exchange rate, P_{770}, is plotted against the alkali-metal polarization obtained for 795 nm pumping at the same spin-exchange rate, P_{795}. (We assume that the Rb and K polarizations are always equilibrated.) The data show the decline in alkali-metal polarization for 795 nm pumping of high-D cells, and also show that P_{770} usually decreases more rapidly with increasing spin-exchange rate as compared to P_{795}. In Fig. 6 is shown the variation of the alkali-metal polarization with spin-exchange rate for 795 and 770 nm pumping of the hybrid Chardonnay (D=1.6) and Syrah cells (D=6.2). For comparison, Fig. 7 shows such data for 795 nm pumping of the pure Rb Chekhov cell and 770 nm pumping of the nearly pure (D=96) K Gigantor cell. Both our experimental determinations of the alkali-metal polarization and calculations of the expected volume-averaged alkali-metal polarization are shown. The calculations were performed by modeling the absorption of laser light in the cell and the resultant position-dependent alkali-metal polarization (see Appendix). For the Chekhov cell, data were obtained with two 795 nm lasers, incident from opposite sides of the oven, providing a total of 52 W of 795 nm laser light. (We did not attempt to modify the calculations to account for light incident from both sides of the cell.) Especially for the pure alkali-metal cells, the data for the alkali-metal polarization are usually lower than the model, in agreement with the earlier observation [37] that the photon efficiency is less than the spin-exchange efficiency.

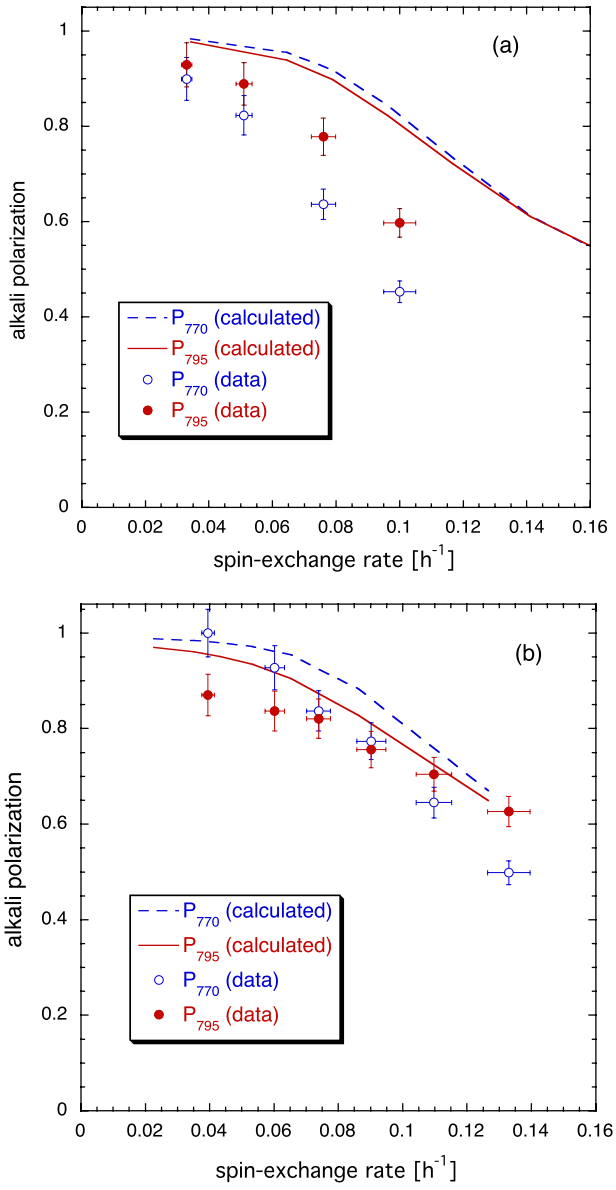

FIG. 6. (Color online) The variation in alkali-metal polarization with spin-exchange rate for both 795 nm (solid circles and solid line) and 770 nm (open circles and dashed line) pumping of (a) the Chardonnay cell (D=1.6) and (b) the Syrah cell (D=6.2). Both experimental determinations (circles) and calculations (lines) of the alkali-metal polarization are shown.

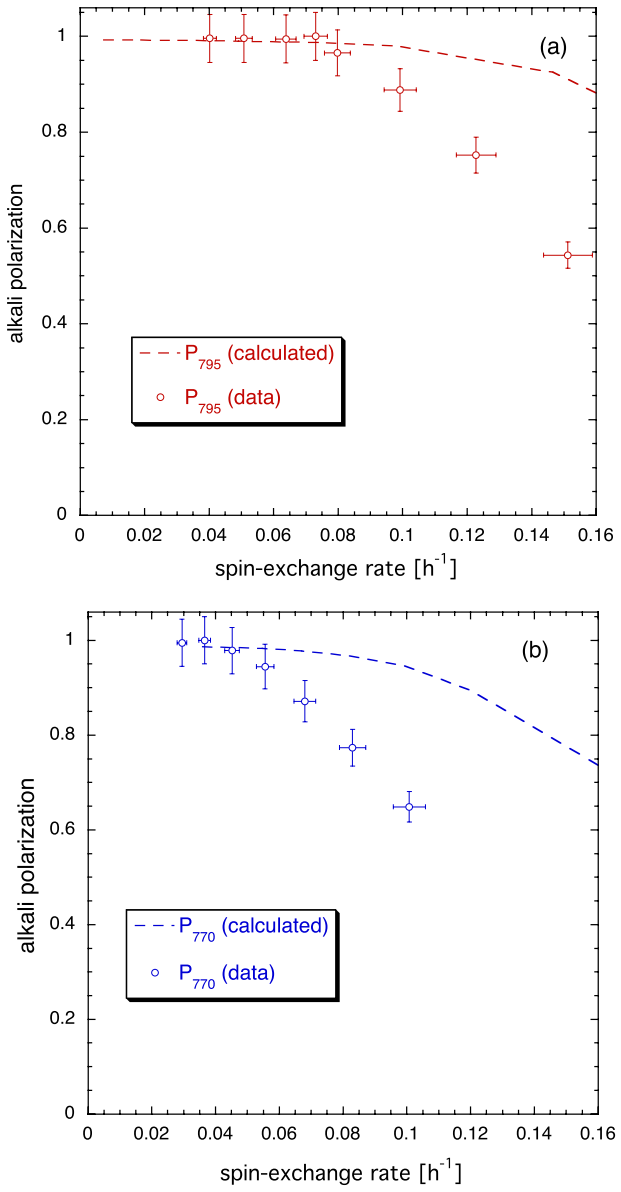

FIG. 7. (Color online) The variation in alkali-metal polarization with spin-exchange rate for (a) 795 nm pumping of the pure Rb Chekhov cell and (b) 770 nm pumping of the nearly pure K Gigantor cell (D=96). Both experimental determinations (open circles) and calculations (dashed lines) of the alkali-metal polarization are shown.

A source of uncertainty in the calculations is the actual laser power incident on the alkali-metal vapor in the cell. The cells used in this study were not designed for accurate measurements of the intensity of the laser light, as they are blown glass cylinders pumped through their side walls. We estimated the loss in intensity due to transmission through two glass oven windows and the cell wall to be 0.78 (4% loss per surface). Although we did include a loss term for absorption by unpolarized alkali-metal on the cell walls [1], we did not include any loss due to imperfect circular polarization of the laser light. Light passing through the curved sides of the cell will suffer some depolarization. We also did not include any loss due to skew light propagation [41], as this is expected to be a minor effect.

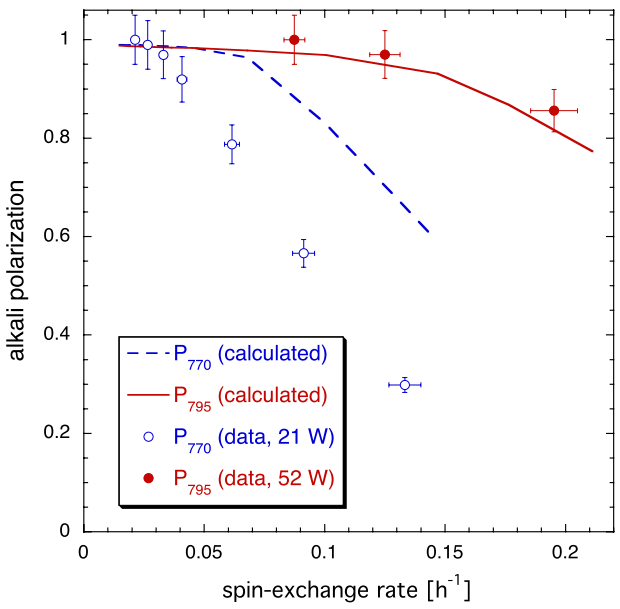

FIG. 8. (Color online) The variation in alkali-metal polarization with spin-exchange rate for optical pumping of the Riesling cell (D=4.8; ^{3}He pressure of 3.5 bar) with 52 W of 795 nm laser light (solid circles and solid line) or with 21 W of 770 nm laser light (open circles and dashed line). Both experimental determinations (circles) and calculations (lines) of the alkali-metal polarization are shown.

It has been proposed that the decline in alkali-metal polarization for large D may be due to off-resonant pumping of potassium atoms by 795 nm light [16]. Using our optical spectrometer [31], we measured the absorption of laser light by a pure K cell between 750 and 840 nm at temperatures up to 520 K. The data follow the expected highly saturated, pressure-broadened, line shape, which yields negligible absorption at 795 nm and thus do not support the assumption of $R_K/R \neq 0$. However, our measurements were not sensitive to the possible existence of a weak, spectrally broad absorption feature. We currently have no other explanation for the behavior of large D cells.

Last, in Fig. 8 we show results for both 795 and 770 nm pumping of the Riesling cell, for which we have obtained the highest polarizing rate (see Sec. IV A). Whereas the data for 795 nm pumping were obtained with 52 W of laser light, we were limited to 21 W of laser light at 770 nm. In both cases, the laser light was incident from both sides of the oven. The performance for 795 nm pumping of this cell actually exceeds the calculation slightly. This behavior was also observed for the Chianti and Barbera cells (data not shown) and is evident to a lesser degree for the Syrah cell (see Fig. 6). In contrast, the data for 770 nm pumping of the Riesling cell are significantly below the calculation, as was typically observed for pure alkali-metal cells and 770 nm pumping, in general. Including the effect of off-resonant absorption of 770 nm light by the K D_2 transition (assuming a pressure-broadened line shape) yields some improvement in the comparison for the Riesling cell, but the effects are smaller at 1 bar and, thus, do not improve the comparisons in our other tests. To summarize, we generally observe the best perfor-

mance and closer agreement with models for 795 nm pumping of hybrid cells, as compared to both 795 nm pumping of pure Rb cells or 770 nm pumping of either pure K or hybrid cells. Further studies are required to understand this observation. From the perspective of practical optical pumping, the results with 795 nm pumping of hybrid cells with D values between 2 and 6 are particularly promising.

V. CONCLUSIONS

We have investigated the efficiency of spin-exchange optical pumping of ^{3}He gas using Rb, Rb-K, and K with spectrally narrowed diode array lasers operating at 795 or 770 nm. We have shown calculations that indicate the practical gain in efficiency for hybrid or pure K SEOP as compared to pure Rb SEOP is a factor of 2 to 4, depending on the cell pressure and vapor density ratio. The predicted gains are lower than those previously reported [16] because we have compared efficiencies at the same spin-exchange rate rather than at the same temperature. When the temperature dependences assumed in our calculations are taken into account, the predicted gains are comparable with those of this earlier work. Our calculations predict lower efficiencies than previously reported measurements for K [13], but the overlap between those data and the practical range of spin-exchange rates we have considered is limited.

We have measured the vapor density ratio in Rb-K hybrid ^{3}He cells using simple absorption of white light and obtained results in good agreement with those obtained from pumping rate measurements, as well as vapor density ratio determinations from the Faraday rotation method [16]. Measurements of the increased efficiency for SEOP of hybrid cells as compared to pure Rb cells, as determined from either the increase in volume that can be polarized or the increase in polarizing rate, yield somewhat better results than calculations. For pressures of 1–2 bar, the improvement in efficiency is typically up to factor of 3, whereas the improvement in polarizing rate is up to a factor of $\approx$1.7. This improvement can be obtained with values of the K-Rb vapor density ratio D between 2 and 6, and in this range we do not observe reduction of the maximum alkali-metal polarization. We also observe that the drop in polarization with increasing polarizing rates is less steep for 795 nm pumping of Rb-K cells as compared to either pure Rb or 770 nm pumping of pure K or Rb-K cells. For 795 nm pumping of pure Rb cells and 770 nm pumping of all cells, our results typically yield photon efficiencies that are lower than spin-exchange efficiencies, but for 795 nm pumping of hybrid cells this effect is less apparent.

For larger vapor density ratios, we observe limited alkali-metal polarization. However, direct measurements of the absorption of white light by a pure K cell indicate that off-resonant absorption due to pressure broadening is negligible. Larger gains are expected at higher pressures, which may provide a more sensitive test of the utility of hybrid and pure K cells. The limited alkali-metal polarization in high-D hybrid cells, even when optically pumped with intense light that should be sufficient to fully polarize the alkali-metal atoms implies that a light-dependent relaxation mechanism of some sort must be present. It seems unlikely that the ^{3}He buffer gas is responsible for this effect.

Our data for the expected improvement in spin-exchange efficiency for hybrid and pure K cells are in reasonable agreement with our calculations, and provide practical evaluation of the utility of Rb-K and pure K optical pumping. However, the discrepancies may indicate issues with the various rate constants and temperature dependences assumed in these calculations. Improved measurements of the temperature dependence of spin-relaxation rates are needed to better estimate the possible gain in efficiency. There might also be inaccuracy in the assumed form of the vapor pressure ratio, for which direct measurements of the alkali-metal densities would be useful.

We have employed two spectrally narrowed 770 nm lasers with linewidths of 0.2–0.26 nm FWHM to optically pump pure K and Rb-K cells. We obtain the same ^{3}He polarization limit of $\approx$75% as has been observed for 795 nm pumping of pure Rb cells and hybrid cells. These results confirm that the alkali-metal polarization is limited for 795 nm pumping of such cells. As expected, we have found that SEOP of pure K at 770 nm is more efficient than SEOP of Rb. In some cases, the gain agreed with calculations but, in other cases, was lower than expected. This may indicate that more careful evaluation of the possible role of off-resonant pumping of the K D_2 transition is required.

Overall, both 795 nm pumping of hybrid cells and 770 nm pumping of pure K and hybrid cells yield similar improvements compared to traditional 795 nm pumping of pure Rb cells. Hybrid cells have the advantage that 795 nm lasers can be employed, but cell filling is complicated by the need to distill two alkali-metals and control the vapor density ratio. The combination of increased laser availability along with the spectral narrowing method makes direct optical pumping of K now possible. In this case, cell filling is simplified. However, the small fine structure splitting makes spectral narrowing particularly important for optical pumping of K. Although we obtained acceptable results using a broadband (1.6 nm FWHM) laser, especially if slightly diminished maximum polarization is acceptable, the achievable polarization is likely to depend strongly on the linewidth and spectrum of the broadband laser.

Our best results were obtained with Rb-K hybrid cells with D between 2 and 6, for which high maximum polarization, high polarizing rate, and decreased sensitivity of the maximum polarization to spin-exchange rate were observed. These cells showed larger improvements compared to pure Rb cells than our calculations predicted. In addition, the slower drop in maximum polarization with increasing spin-exchange rate was an unexpected benefit of substantial practical utility. Using 52 W of spectrally narrowed laser light at 795 nm, we have produced 75% polarized ^{3}He gas at a rate of 2.4 bar l/d or 50% polarized ^{3}He gas at a rate of 10.5 bar l/d. We plan studies of higher pressure cells, for which optimized hybrid cells should yield further improvements in performance.

ACKNOWLEDGMENTS

Special acknowledgement goes to J. Anderson and J. Fuller of the NIST Optical Shop for construction of the cells used in this work. We also thank W. Hersman for loan of the cell NHRbK. This work was supported in part by the Department of Energy, Basic Energy Sciences.

APPENDIX: ALKALI POLARIZATION MODEL

The model employed assumes that the alkali-metal polarization $P_A(z)$ at any given location z along the laser beam axis is given by

$$P_A(z) = \frac{R(z)}{R(z) + \Gamma_A}, \tag{A1}$$

where $R(z)$ is the optical pumping rate at that location. $R(z)$ is given by

$$R(z) = \int \phi(z,\nu)\sigma_A(\nu)\mathrm{d}\nu \tag{A2}$$

where $\phi(z,\nu)$ is the number of photons per unit area per unit time in the frequency interval $\mathrm{d}\nu$ at a given z and ν, and $\sigma_A(\nu)$ is the frequency-dependent optical absorption cross section. $\sigma_A(\nu)$ was assumed to have a Lorentzian form,

$$\sigma_A(\nu) = \frac{\sigma_{A0}}{1 + 4\Delta^2/\gamma_A^2}, \tag{A3}$$

where σ_{A0} is the peak cross section, $\Delta = \nu - \nu_0$ is the frequency offset from the optical pumping resonant frequency ν_0, and γ_A is the pressure broadened width for the D_1 transition of either Rb or K. At a pressure of one bar (temperature of 296 K), $\sigma_{\mathrm{Rb0}} = 3.2 \times 10^{-13}$ cm $\sigma_{\mathrm{K0}} = 4.5 \times 10^{-13}$ cm^2, $\gamma_{\mathrm{Rb0}} = 17.2$ GHz [40], and $\gamma_{\mathrm{K0}} = 12.1$ GHz [39]. A Lorentzian form was also assumed for $\phi(z,\nu)$, with the measured widths. The total photon flux was estimated from the measured laser power incident on the oven, and the size of the rectangular beam spot at the cell. The optical pumping rate at a location $z + \Delta z$ is determined from the absorption of circularly polarized light in the distance Δz,

$$\phi(z + \Delta z, \nu) = \phi(z,\nu)\exp\{-[A]\sigma(\nu)[1 - P_\infty P_A(z)]\Delta z\}. \tag{A4}$$

Since the cells are side pumped, the total distance through the cell is not constant; the model included a volume average for the alkali-metal polarization with the assumption of a cylindrical cell. A loss term for absorption by unpolarized alkali-metal on the cell walls [1] was included.

[1] T. G. Walker and W. Happer, Rev. Mod. Phys. **69**, 629 (1997).
[2] M. A. Bouchiat, T. R. Carver, and C. M. Varnum, Phys. Rev. Lett. **5**, 373 (1960).
[3] T. R. Gentile *et al.*, Physica B **356**, 96 (2005); T. Ino *et al.*, *ibid.* **356**, 109 (2005); G. W. Wallidge *et al.*, *ibid.* **356**, 118 (2005); Y. S. Lee, G. Kim, V. R. Skoy, and T. Ino, J. Korean Phys. Soc. **48**, 233 (2006).
[4] T. R. Gentile, W. C. Chen, G. L. Jones, E. Babcock, and T. G. Walker, J. Res. Natl. Inst. Stand. Technol. **110**, 299 (2005).
[5] K. P. Coulter *et al.*, Nucl. Instrum. Methods Phys. Res. A **270**, 90 (1988).
[6] X. Zheng *et al.*, Phys. Rev. C **70**, 065207 (2004).
[7] T. Katabuchi *et al.*, Rev. Sci. Instrum. **76**, 033503 (2005).
[8] E. J. R. van Beek *et al.*, J. Magn. Reson Imaging **20**, 540 (2004); M. S. Albert *et al.*, Nature (London) **370**, 199 (1994).
[9] M. Batz *et al.*, J. Res. Natl. Inst. Stand. Technol. **110**, 293 (2005).
[10] J. Becker *et al.*, Nucl. Instrum. Methods Phys. Res. A **346**, 45 (1994).
[11] F. D. Colegrove, L. D. Schearer, and G. K. Walters, Phys. Rev. **132**, 2561 (1963).
[12] T. G. Walker, J. H. Thywissen, and W. Happer, Phys. Rev. A **56**, 2090 (1997).
[13] A. B. Baranga, S. Appelt, M. V. Ronalis, C. J. Erickson, A. R. Young, G. D. Cates, and W. Happer, Phys. Rev. Lett. **80**, 2801 (1998).
[14] G. Wang, W. Shao, and E. W. Hughes, Phys. Rev. A **68**, 065402 (2003).
[15] W. Happer, G. D. Cates, M. V. Romalis, and C. J. Erickson, U.S. Patent No. 6,318,092 (2001).
[16] E. Babcock, I. Nelson, S. Kadlecek, B. Driehuys, L. W. Anderson, F. W. Hersman, and T. G. Walker, Phys. Rev. Lett. **91**, 123003 (2003).
[17] B. Chann, I. Nelson, and T. G. Walker, Opt. Lett. **25**, 1352 (2000).
[18] B. Chann, E. Babcock, L. W. Anderson, and T. G. Walker, Phys. Rev. A **66**, 032703 (2002).
[19] E. Babcock, Ph. D. thesis, University of Wisconsin, Madison, 2005.
[20] D. Lide, *Handbook of Chemistry and Physics*, 85th ed. (CRC Press, Boca Raton, 2004).
[21] See for example, J. E. Brady and G. E. Humiston, *General Chemistry: Principles and Structure* (Wiley, New York, 1975).
[22] S. Kadlecek, Ph.D. thesis, University of Wisconsin, Madison, (2000).
[23] I. A. Nelson and T. G. Walker, Phys. Rev. A **65**, 012712 (2001).
[24] T. G. Walker, I. Nelson, and S. Kadlecek, Amersham Health Report (unpublished).
[25] D. R. Rich, T. R. Gentile, T. B. Smith, A. K. Thompson, and G. L. Jones, Appl. Phys. Lett. **80**, 2210 (2002).
[26] GE Lighting Component Sales, Bldg. 315D, 1975 Noble Rd., Cleveland, OH 44117. Certain trade names and company products are mentioned in the text or identified in an illustration in order to adequately specify the experimental procedure and equipment used. In no case does such identification imply recommendation or endorsement by the National Institute of Stan-

dards and Technology, nor does it imply that the products are necessarily the best available for the purpose.
[27] L. Liew *et al.*, Appl. Phys. Lett. **84**, 2694 (2004).
[28] X. Zeng, Z. Wu, T. Call, E. Miron, D. Schreiber, and W. Happer, Phys. Rev. A **31**, 260 (1985).
[29] B. Chann *et al.*, J. Appl. Phys. **94**, 6908 (2003).
[30] Quintessence Photonics Corporation, 15632 Roxford Street, Sylmar, CA 91342-1265.
[31] Ocean Optics Inc., 380 Main Street, Dunedin, FL 34698.
[32] Coherent Semiconductor Group, 5100 Patrick Henry Dr., Santa Clara, CA 95054.
[33] nLight Corporation, 408 NE 88th Street, Bldg. E, Vancouver, WA 98665.
[34] W. Happer *et al.*, Rev. Mod. Phys. **44**, 169 (1972).
[35] The cell NHRbK was employed for the work reported in Ref. [16], and was originally provided by W. Hersman.
[36] J. Migdalek and Y. Kim, J. Phys. B **31**, 1947 (1998).
[37] E. Babcock, B. Chann, T. G. Walker, W. C. Chen, and T. R. Gentile, Phys. Rev. Lett. **96**, 083003 (2006).
[38] D. K. Walter, W. M. Griffith, and W. Happer, Phys. Rev. Lett. **86**, 3264 (2001).
[39] N. Allard and J. Kielkopf, Rev. Mod. Phys. **54**, 1103 (1982); N. Lwin and D. G. McCartan, J. Phys. B **11**, 3841 (1978).
[40] M. V. Romalis, E. Miron, and G. D. Cates, Phys. Rev. A **56**, 4569 (1997).
[41] B. Chann, E. Babcock, L. W. Anderson, and T. G. Walker, Phys. Rev. A **66**, 033406 (2002).